INSTITUTE OF PHYSICS PUBLISHING JOURNAL OF PHYSICS: CONDENSED MATTER

J. Phys.: Condens. Matter **18** (2006) S1039–S1047 doi:10.1088/0953-8984/18/25/S10

Numerical study of pressure relationships between sample and calibrant inside the diamond anvil cell

Nathalie Conil and Abby Kavner

Earth and Space Science Department and Institute for Geophysics and Planetary Physics, University of California, Los Angeles, 595 Charles Young Drive East, Los Angeles, CA 90095, USA

Received 13 January 2006, in final form 19 April 2006
Published 8 June 2006
Online at stacks.iop.org/JPhysCM/18/S1039

Abstract

We present isotropic, elastic–plastic finite element calculations detailing the pressure relationship between an inclusion and its surrounding matrix, subject to an externally imposed hydrostatic strain. In general, the inclusion and the matrix have different values of hydrostatic pressure, depending on their absolute and relative values of Young's modulus and Poisson's ratio. A series of finite element models was used to explore the parameter space of the elastic and plastic properties of an inclusion within a matrix. In all cases where there is insufficient relaxation of the nonhydrostatic stress, the material with the higher bulk modulus will also have a higher pressure, regardless of the shear moduli. The complete data set was subjected to a Pareto analysis to determine the main and secondary effects which influence the final result, expressed as the ratio of the pressure of the matrix to that of the inclusion. The four most important factors which determine the pressure ratio of an inclusion and matrix are the Young's modulus of the matrix, the interaction of the Young's modulus and the yield strength of the matrix material, the Young's modulus of the inclusion, and the interaction of the Young's modulus of the inclusion with the yield strength of the matrix material. The yield strength of the inclusion has a statistically insignificant effect on the results. This information provides guidelines for designing the most effective combinations of unknowns and material standards to minimize pressure errors in equation of state measurements.

1. Introduction

The development of synchrotron capabilities has accelerated the ability to perform *in situ* measurements of the equation of state and phase stability of deep Earth minerals at the relevant pressure and temperature conditions. Many of the measurements rely on the ability to measure x-ray diffraction information from two materials together within a high pressure sample chamber—an unknown material of interest, and a standard material with a well-characterized equation of state to be used as a pressure calibrant. For example, a study by Irifune *et al* (1998) shows that the ringwoodite/perovskite transformation in Mg_2SiO_4, long thought to be responsible for

the 660 km discontinuity, actually transforms at a pressure of 21 GPa, 2 GPa lower than the observed seismic boundary. However, in a series of alternate experiments performed in the laser heated diamond cell (Hirose *et al* 2001a, 2001b, Shim *et al* 2001, Chudinovskikh and Boehler 2004) the presence of the phase transformation at pressures corresponding to the seismic discontinuity was confirmed. Since all of these experiments require samples which mix calibrated standards with the material of interest, the cumulative experimental results suggest inconsistencies in the calibrations of standard materials which act as *in situ* pressure markers. These, and other similar results, have sparked a significant community-wide effort to examine the high temperature, high pressure equation of state of standard materials including Au, MgO, Pt Re, and others; see for example (Shim *et al* 2002, Fei *et al* 2004).

These studies have shown that errors in the high P, T equation of state can be responsible for many of the pressure discrepancies in the literature. One potential cause of the errors in the equation of state measurements has been identified as the presence of nonhydrostatic stresses within the sample chamber. In the x-ray geometry that is normally used for lattice strain measurements, from which equation of state information is derived, the presence of even small amounts of nonhydrostatic stress can severely underestimate the volumetric lattice strains, resulting in too high values of bulk modulus (e.g. Kavner *et al* 2000). Accurate assessments of equations of state using this x-ray geometry require a fully hydrostatic sample environment. Two methods have been used to maintain this condition: gas loading the sample within a perfectly hydrostatic medium, and laser annealing. The goal of gas loading is to create isolated grains fully surrounded by a liquid environment in the high pressure sample chamber, and there has been a recent focus of effort on this. However, radial diffraction measurements from argon, a commonly used pressure medium, have shown that this material can support significant amounts of nonhydrostatic stress (Mao H K *et al*, personal communication). H and He are significantly more difficult to load in the sample chamber without specialized equipment. Laser heating is also used to 'anneal' the nonhydrostatic component of the stresses within the sample. However, a study following the high P, T behaviour of two materials mixed together in the diamond anvil cell shows that significant nonhydrostatic stress may be reintroduced into the sample during the rapid thermal quench as the laser is shut off; and there may even be differential stress present at high temperatures, especially in the presence of steep temperature gradients (Kavner and Duffy 2001).

Further difficulties are introduced when two materials are mixed together within the high pressure environment. The usual assumption made in this case is that the pressures of the two phases are equal. However, this will only be the case if all of the elastic shear stresses are able to relax on the timescale of the experiment. There have been some enquiries into the stress state in a sample chamber where two materials are mixed together. Wang *et al* (1998) pointed out that inclusions in a matrix may suffer from stress gradients near the interface, resulting in pressure differences inferred from x-ray diffraction strain measurements. However, there has not yet been a quantitative analysis of this effect, applied across a series of sample environments.

In this study, we used a finite element code to analyse the pressure relationships of an inclusion within a matrix in the diamond cell sample chamber, and applied a Pareto analysis to extract the most significant variables affecting the pressure relationship. The goal of these calculations was to simulate an idealized condition where the externally applied stresses are purely hydrostatic. The corresponding idealized diamond cell experiment would be a sample consisting of oxide or silicate with pressure-marker inclusions, surrounded by a perfectly fluid medium such as He. In most real situations, the stress state in the diamond cell sample chamber likely deviates from hydrostaticity. Therefore, in addition to the idealized system, we analyse analogous experimental systems from our own research and others, to generate a prediction of potential pressure pitfalls in the diamond anvil cell.

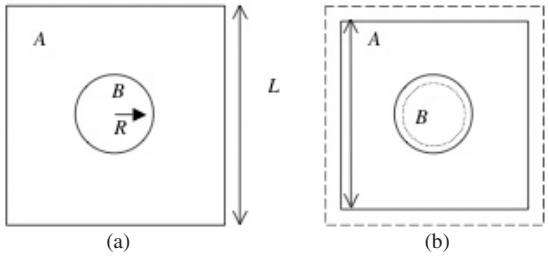

Figure 1. Sample geometry for the two-dimensional cases of inclusion (B) embedded in a matrix (A); (a) before compression (b) after hydrostatic displacement.

2. Method

We performed a series of finite element calculations on an inclusion within a matrix subject to an externally applied hydrostatic stress using the commercially available finite element code, Zebulon (Northwest Numerics). The geometry for all samples consists of a square solid S constituted by two phases: the matrix, A, which surrounds one inclusion B (figure 1). The starting linear size ratio of the inclusion to the matrix was 0.2. The study was performed in two dimensions. For the purposes of this study, we use a time-independent, isotropic, linearly elastic/perfectly plastic mechanical model for the behaviour of both matrix and inclusion. Each phase is assumed to be continuous with homogeneous properties. Therefore, each material is characterized by three independent parameters: two elastic moduli and a yield stress following the von Mises yield criterion (yielding occurs when the differential stress exceeds the yield stress). In the elastic domain we considered E_{A} and E_{B}, the Young's modulus for the phase A and the phase B, respectively, and ν_{A} and ν_{B}, the Poisson ratios. Elastic deformations occur as long as stresses do not exceed the yield strength of the phase, σ_{yA} and σ_{yB}. Once the yield strength thresholds are reached, they can deform plastically, or flow.

The procedure used in the finite element program is based on an incremental stress and strain analysis. Below a shear modulus yield criterion, we increment the elastic strain, and solve for stress using Hooke's law for an isotropic solid:

$$\underline{\underline{\rho}} = E\underline{\underline{\varepsilon}}^{\mathrm{e}} \tag{1}$$

where σ is the stress tensor, E is the Young's modulus, and ε^{e} is the elastic portion of the strain. For an isotropic solid, there are two independent elastic moduli, Young's modulus, E, and Poisson's ratio, ν. However, the yield criterion is based on a maximum shear modulus, G. To calculate G, the relationship used is given by

$$G = \frac{E}{2(1+\nu)}. \tag{2}$$

Above the yield strength, the strain is no longer elastic, but is perfectly plastic (no increase of stress with increasing strain). The total strain is the elastic portion plus the plastic portion, written as

$$d\underline{\underline{\varepsilon}} = d\underline{\underline{\varepsilon}}^{\mathrm{e}} + d\underline{\underline{\varepsilon}}^{\mathrm{p}} \tag{3}$$

where $d\underline{\underline{\varepsilon}}^{\mathrm{e}}$ is the elastic strain increment, related to the stress increment by the classical Hooke's law in a isotropic case. $d\underline{\underline{\varepsilon}}^{\mathrm{p}}$ is the plastic strain increment. Our calculations are carried out with the composite sample geometry outlined in figure 1. L is the length of the side of the square and R the radius of the inclusion. A constant displacement boundary conditions was applied at the inclusion/matrix boundary. To generate a hydrostatic loading we applied the same displacement

on the edges of the sample $U = U_1 = U_2$. The output of the program was an evaluation of the stress state within each element, which was then averaged separately in the inclusion and the matrix, in terms of its hydrostatic and differential components. Most of the stress redistribution occurred near the inclusion/matrix boundary.

2.1. Design and statistical analysis of experiments

A full table of variable response was run (table 1), perturbing each of the six experimental variables (E_A, E_B, ν_A, ν_B, σ_{yA}, σ_{yB}) between low and high limits representing a wide range of conceivable values (table 1). A total of 64 separate models were run. A Pareto analysis of the variable response was performed using the commercial software Minitab (www.minitab.com). A Pareto analysis is a formal technique in statistical analysis which quantifies how variations in each parameter influence the final outcome, when many variables are involved. The Pareto analysis ranks the relative influence of each variable on the designated outcome variable, all other things being equal (statistically). In this case, we choose the outcome variable to be the pressure ratio between the sample and inclusion, P_A/P_B. An important assumption that is made in this Pareto analysis is that the outcome (P_A/P_B) is a linear response of each input variable, which allows the use of high and low limits of each variable. This assumption was tested by several models which employed intermediate values, as a check that the outcome was also proportionally intermediate.

3. Results and discussion

Table 1 shows the list of input parameters for each numerical model, and the resulting pressure ratio between the matrix and inclusion is given in the last column. These results show that, in general, the pressure of an inclusion and a matrix are not equal, even when the composite material is subject to an externally imposed hydrostatic displacement.

The Pareto chart created by Minitab (figure 2) provides a graphic summary of the relative importance in each of the variables in determining the final outcome of the data (P_A/P_B). The Pareto analysis can also be employed to generate a list of interaction effects—how two parameters combine to determine the outcome. The analysis performed here also included two-way and three-way interactions among the individual parameters (figure 2).

The single most significant determinator of the pressure difference between the matrix and the inclusion is the Young's modulus of the matrix, E_A (A in figure 2). This is the most important single parameter in determining the relative pressure between the matrix and the inclusion; and the two-way interaction of the Young's modulus and the yield strength of the matrix has an equivalent influence on the outcome of the models. The next two most important effects encompass the Young's modulus of the inclusion: that variable alone is the third most important determinator of the pressure difference, and the interaction with the yield strength of the matrix is the next most important. These four effects comprise the most important relationships between composite sample properties and resulting pressure ratios.

The Poisson's ratio of the inclusion shows up as the fifth-ranked important variable, and as the sixth-ranked variable, in combination with the yield strength of the inclusion. The lack of combined Poisson's ratio/Young's modulus (AC and BD) effects in the top ten attests to the importance of a material's Young's modulus relative to either the bulk or shear modulus, in determining its pressure response. Since bulk and shear moduli are linear combinations of Young's and Poisson's values, these interaction effects would be more important if the bulk and shear moduli controlled the sample behaviour. For example, even though the Young's modulus of the matrix is the single most important variable, the corresponding Poisson's ratio does not

Table 1. Full table of models—hydrostatic, inclusion case.

Run	E_A	E_B	ν_A	ν_B	σ_{yA}	σ_{yB}	P_A/P_B	K_A	K_B
1	300	300	0.45	0.45	8	8	1	10	10
2	300	300	0.45	0.45	8	0.01	1.002	10	10
3	300	300	0.45	0.45	0.01	8	0.1	10	10
4	300	300	0.45	0.45	0.01	0.01	1	10	10
5	300	300	0.45	0.25	8	8	1.147	10	50
6	300	300	0.45	0.25	8	0.01	1.148	10	50
7	300	300	0.45	0.25	0.01	8	1.001	10	50
8	300	300	0.45	0.25	0.01	0.01	1.000	10	50
9	300	300	0.25	0.45	8	8	0.836	50	10
10	300	300	0.25	0.45	8	0.01	0.677	50	10
11	300	300	0.25	0.45	0.01	8	0.999	50	10
12	300	300	0.25	0.45	0.01	0.01	0.999	50	10
13	300	300	0.25	0.25	8	8	1	50	50
14	300	300	0.25	0.25	8	0.01	1.034	50	50
15	300	300	0.25	0.25	0.01	8	0.1	50	50
16	300	300	0.25	0.25	0.01	0.01	1	50	50
17	300	50	0.45	0.45	8	8	1.165	10	1.667
18	300	50	0.45	0.45	8	0.01	1.165	10	1.667
19	300	50	0.45	0.45	0.01	8	1.001	10	1.667
20	300	50	0.45	0.45	0.01	0.01	1.001	10	1.667
21	300	50	0.45	0.25	8	8	1.472	10	8.333
22	300	50	0.45	0.25	8	0.01	1.509	10	8.333
23	300	50	0.45	0.25	0.01	8	1.005	10	8.333
24	300	50	0.45	0.25	0.01	0.01	1.002	10	8.333
25	300	50	0.25	0.45	8	8	1.083	50	1.667
26	300	50	0.25	0.45	8	0.01	1.094	50	1.667
27	300	50	0.25	0.45	0.01	8	1.000	50	1.667
28	300	50	0.25	0.45	0.01	0.01	1.000	50	1.667
29	300	50	0.25	0.25	8	8	1.846	50	8.333
30	300	50	0.25	0.25	8	0.01	1.982	50	8.333
31	300	50	0.25	0.25	0.01	8	1.003	50	8.333
32	300	50	0.25	0.25	0.01	0.01	1.002	50	8.333
33	50	300	0.45	0.45	8	8	0.922	1.667	10
34	50	300	0.45	0.45	8	0.01	0.923	1.667	10
35	50	300	0.45	0.45	0.01	8	0.999	1.667	10
36	50	300	0.45	0.45	0.01	0.01	0.999	1.667	10
37	50	300	0.45	0.25	8	8	0.975	1.667	50
38	50	300	0.45	0.25	8	0.01	0.987	1.667	50
39	50	300	0.45	0.25	0.01	8	1	1.667	50
40	50	300	0.45	0.25	0.01	0.01	1	1.667	50
41	50	300	0.25	0.45	8	8	0.837	8.333	10
42	50	300	0.25	0.45	8	0.01	0.677	8.333	10
43	50	300	0.25	0.45	0.01	8	0.997	8.333	10
44	50	300	0.25	0.45	0.01	0.01	0.998	8.333	10
45	50	300	0.25	0.25	8	8	0.72	8.333	50
46	50	300	0.25	0.25	8	0.01	0.731	8.333	50
47	50	300	0.25	0.25	0.01	8	0.997	8.333	50
48	50	300	0.25	0.25	0.01	0.01	0.998	8.333	50
49	50	50	0.45	0.45	8	8	1	1.667	1.667
50	50	50	0.45	0.45	8	0.01	1.003	1.667	1.667
51	50	50	0.45	0.45	0.01	8	1	1.667	1.667
52	50	50	0.45	0.45	0.01	0.01	1	1.667	1.667

Table 1. (Continued.)

Run	E_A	E_B	ν_A	ν_B	σ_{yA}	σ_{yB}	P_A/P_B	K_A	K_B
53	50	50	0.45	0.25	8	8	1.309	1.667	8.333
54	50	50	0.45	0.25	8	0.01	1.388	1.667	8.333
55	50	50	0.45	0.25	0.01	8	1.002	1.667	8.333
56	50	50	0.45	0.25	0.01	0.01	1.001	1.667	8.333
57	50	50	0.25	0.45	8	8	0.742	8.333	1.667
58	50	50	0.25	0.45	8	0.01	0.744	8.333	1.667
59	50	50	0.25	0.45	0.01	8	0.997	8.333	1.667
60	50	50	0.25	0.45	0.01	0.01	0.998	8.333	1.667
61	50	50	0.25	0.25	8	8	1	8.333	8.333
62	50	50	0.25	0.25	8	0.01	1.067	8.333	8.333
63	50	50	0.25	0.25	0.01	8	0.999	8.333	8.333
64	50	50	0.25	0.25	0.01	0.01	1	8.333	8.333

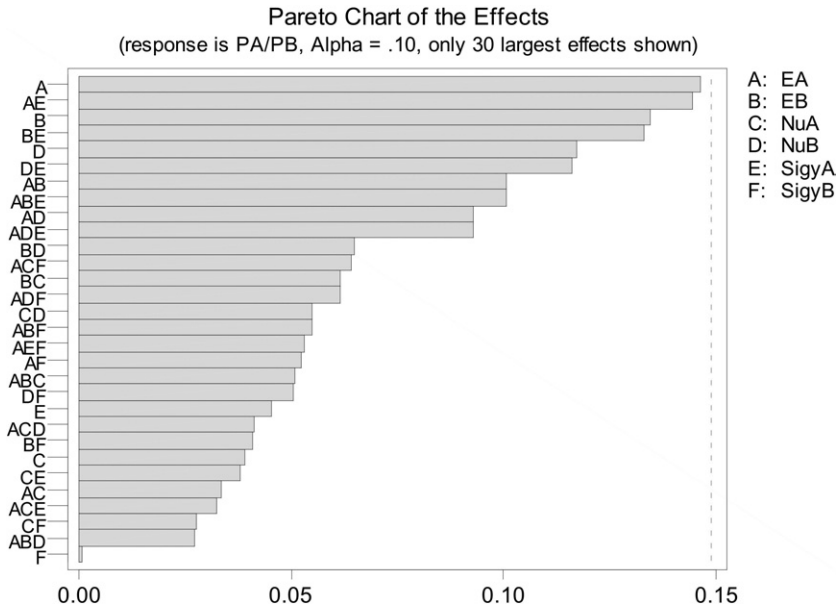

Figure 2. A Pareto chart showing the relative influence of each variable (legend in the figure) on the final outcome of the numerical models (P_A/P_B). One-way, two-way, and three-way variable interactions are shown.

show up until the 12th most important influence, and then, only in a three-way combination with the matrix Young's modulus, and the yield strength of the inclusion.

By itself, the yield strength of either the matrix or the inclusion did not have a significant effect on the pressure difference. The yield strength of the matrix was only important in its interaction with the Young's modulus of the matrix and, to a lesser extent, but still significant, the inclusion. To our extreme surprise, the yield strength of the inclusion, σ_B (parameter F in figure 2), had almost no effect on the pressure outcome. That by itself suggests that the high strength of Pt relative to Au (Duffy *et al* 1999a, 1999b, Kavner and Duffy 2003) will not play a significant role in generating a pressure variation in samples which use these materials as a mixed-in pressure marker. However, this also means that the relatively low yield strength of these calibrant materials cannot help to ensure a hydrostatic environment.

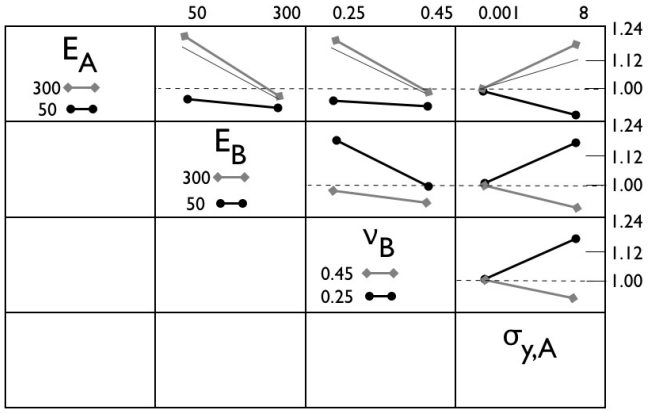

Figure 3. A Pareto chart showing the important two-way interactions among the variables. The interactions are between the variables in the rows (E_A, E_B, ν_B) and the columns (E_B, ν_B, $\sigma_{y,A}$). The final outcome of the numerical models (P_A/P_B) is shown on the right. The horizontal dotted lines along each row designate the condition (P_A/P_B) = 1. The thin grey lines in the first row represent a sample with a Young's modulus of 280 GPa.

Laser heating has been suggested as a means to anneal pressure differences and nonhydrostaticity in high pressure samples (Jackson *et al* 2004, Sinogeikin *et al* 2004a, 2004b). Heating can only relax the yield strength, and we found in these results that the yield strength plays a secondary role in determining the pressure discontinuity between an inclusion and its surrounding matrix. Heating samples, if done uniformly, does serve to relax most deviatoric stress, due to the loss of strength of materials as the homologous temperature (T/T_m) increases. Of course, the ability of heating to restore a hydrostatic environment depends on the relationship of the temperature to the melting temperature (high T_m materials will require larger temperatures to relax deviatoric stresses) and uniformity of temperatures. It is unclear how large temperature gradients in the diamond cell combined with fast quench times affect large-scale stress heterogeneity, especially in the case of inclusions.

4. Sample design for equation of state and phase stability measurements

The ultimate goal of experiments to determine the equation of state and/or phase stability at high pressures is to ensure as hydrostatic an environment as possible. However, this is not always possible, for several potential reasons. There are only a limited number of truly hydrostatic media, and the desire to reproduce results under different loading conditions means that a hydrostatic loading environment might not be available. Furthermore, hydrostaticity is increasingly difficult to maintain under increasingly extreme conditions. At high pressures, hydrostaticity may be lost due to large volume shrinkage of hydrostatic media with respect to the (usually) less compressible sample; and at high temperatures, stress gradients may be associated with temperature gradients. When hydrostaticity is not guaranteed, the next best choice is to attempt to ensure that any pressure difference between the matrix and the inclusion is minimized. The interaction Pareto chart (figure 3) can be used as a guide to formulating experiments. The chart shows the most important two-way interactions among four variables: E_A, E_B, ν_B and $\sigma_{y,A}$. Together, these variables account for 11 out of the top 12 influences on pressure relationships between the sample and the inclusion.

For example, the dotted horizontal lines along each row in figure 3 show the elastic property requirements for the pressure of the inclusion to be equal to that of the matrix. The

first row of the plot in figure 3 shows how the Young's modulus of the matrix combines with the Young's modulus of the inclusion (second column), Poisson's ratio of the inclusion (third column), and the yield strength of the matrix (fourth column) to influence the pressure difference between the matrix and the inclusion (right-hand axis). In the first row, the two plotted thick lines correspond to the two end members of E_A, the Young's modulus of the matrix (50 and 300 GPa). For this example, we assume that the matrix has a Young's modulus of 285 GPa and a Poisson's ratio of 0.255. These are approximately the isotropic elastic constants for the mineral ringwoodite, at ambient pressures and temperatures (Sinogeikin *et al* 2001). First, a line corresponding to E_A of our sample material is interpolated between the two end members. This linear interpolation is shown as thin grey lines in the first row of figure 3. The point on the X-axis where this interpolated line intersects the dotted line corresponding to $P_A/P_B = 1$ describes the design criteria for the value shown in each column. For example, in the second column, the interpolated line intersects $P_A/P_B = 1$ at an X-axis value that is significantly lower than $E_B = 285$—closer to $E_B = 250$ GPa. Therefore, an inclusion with a Young's modulus about 12% smaller than the matrix will have the greatest effect in helping to ensure uniform pressures. The third column shows how the interactions between the matrix Young's modulus and the inclusion poisson value influences pressure. In this case, an inclusion with a high Poisson's ratio—about 0.4—will help maintain pressure equality. Finally, the last column shows simply the fundamental effect of sample strength. The pressure relationship is always unity when the yield strength of the matrix approaches zero.

This analysis provides a first order accounting of the pressure differences for phase transformations in ringwoodite using Au as a pressure marker (Irifune *et al* 1998) versus Pt (Shim *et al* 2001). Both Au and Pt have similar values of the Poisson's ratio—0.4—which is the proper value to minimize their effects on pressure differences. However, Young's modulus of Pt, 179 GPa, is much larger than that for Au, 78.5 GPa. Therefore, it makes sense that the large mismatch between the Young's modulus of the ringwoodite sample and a gold inclusion could cause a pressure mismatch within the high pressure sample chamber.

5. Conclusions

This model was designed to be a simple, straightforward approach to examining the most important influences on pressure relationships in samples in a high pressure sample chamber. In a future set of models, some of the next analyses to include will be: a more realistic strain-hardening rheology of sample response, an examination of interactions between neighbouring inclusions, examination of size effects of inclusions, and an extension of this analysis to include polycrystalline samples. These can be modelled by approaching them as a composite of randomly oriented materials with different elastic and plastic properties. This problem can be approached using two basic stages of complexity. In a simple model, elastic and plastic properties change with grain orientation for input polycrystalline material, but each grain has constant properties. In a more complicated model, the elastic and plastic properties of each individual grain change at each displacement step, and change with rotation of the grain within the matrix (Korsunsky *et al* 2000).

Our goal was to determine the pressure and the elastic strain component of each phase, to study the influence of both elastic parameters (Young's modulus and Poisson's ratio) and the yield strength on the relative pressure of inclusion and matrix. Both the elastic and strength properties of both the matrix and the inclusion help determine the relative pressure between the two. The Pareto analysis quantifies the relative importance of each of these variables—acting singly and in tandem—in determining the pressure difference. The most important outcome is that the pressure difference between the matrix and the inclusion is to first order related to the

Young's modulus of the matrix, and a combination of Young's modulus and yield strength of the matrix. The Young's modulus of the inclusion is the third most important variable, and its combination with the matrix yield strength is the next most important. Taken together, these results can point the ways towards intelligent design of composite samples to optimize equation of state measurements in the diamond anvil cell and other high pressure sample environments.

Acknowledgment

This work was performed with help from NSF grant EAR 0440332.

References

Chudinovskikh L and Boehler R 2004 $MgSiO_3$ phase boundaries measured in the laser-heated diamond cell *Earth Planet. Sci. Lett.* **219** 285–96

Duffy T S, Shen G Y, Heinz D L, Shu J F, Ma Y Z, Mao H K, Hemley R J and Singh A K 1999a Lattice strains in gold and rhenium under nonhydrostatic compression to 37 GPa *Phys. Rev.* B **60** 15063–73

Duffy T S, Shen G Y, Shu J F, Mao H K, Hemley R J and Singh A K 1999b Elasticity, shear strength, and equation of state of molybdenum and gold from x-ray diffraction under nonhydrostatic compression to 24 GPa *J. Appl. Phys.* **86** 6729–36

Fei Y, Van Orman J, Li J, van Westrenen W, Sanloup C, Minarik W, Hirose K, Komabayashi T, Walter M and Funakoshi K 2004 Experimentally determined postspinel transformation boundary in Mg_2SiO_4 using MgO as an internal pressure standard and its geophysical implications *J. Geophys. Res.-Solid Earth* **109** B02305

Hirose K, Fei Y W, Ono S, Yagi T and Funakoshi K 2001a In situ measurements of the phase transition boundary in $Mg_3Al_2Si_3O_{12}$: implications for the nature of the seismic discontinuities in the Earth's mantle *Earth Planet. Sci. Lett.* **184** 567–73

Hirose K, Komabayashi T, Murakami M and Funakoshi K 2001b *In situ* measurements of the majorite–akimotoite–perovskite phase transition boundaries in $MgSiO_3$ *Geophys. Res. Lett.* **28** 4351–4

Irifune T, Nishiyama N, Kuroda K, Inoue T, Isshiki M, Utsumi W, Funakoshi K, Urakawa S, Uchida T, Katsura T and Ohtaka O 1998 The postspinel phase boundary in Mg_2SiO_4 determined by *in situ* x-ray diffraction *Science* **279** 1698–700

Jackson J M, Zhang J and Bass J D 2004 Sound velocities and elasticity of aluminous $MgSiO_3$ perovskite: implications for aluminum heterogeneity in the Earth's lower mantle *Geophys. Res. Lett.* **31** L10614

Kavner A and Duffy T S 2001 Pressure–volume–temperature paths in the laser-heated diamond anvil cell *J. Appl. Phys.* **89** 1907–14

Kavner A and Duffy T S 2003 Elasticity and rheology of platinum under high pressure and nonhydrostatic stress *Phys. Rev.* B **68**

Kavner A, Sinogeikin S V, Jeanloz R and Bass J D 2000 Equation of state and strength of natural majorite *J. Geophys. Res.-Solid Earth* **105** 5963–71

Korsunsky A M, Daymond M R and Wells K E 2000 The development of strain anisotropy during plastic deformation of an aluminium polycrystal *Ecrs 5: Proc.5th European Conf. on Residual Stresses* pp 492–7

Shim S H, Duffy T S and Kenichi T 2002 Equation of state of gold and its application to the phase boundaries near 660 km depth in Earth's mantle *Earth Planet. Sci. Lett.* **203** 729–39

Shim S H, Duffy T S and Shen G Y 2001 The post-spinel transformation in Mg_2SiO_4 and its relation to the 660-km seismic discontinuity *Nature* **411** 571–4

Sinogeikin S V, Bass J D and Katsura T 2001 Single-crystal elasticity of gamma-$(Mg_{0.91}Fe_{0.09})_2SiO_4$ to high pressures and to high temperatures *Geophys. Res. Lett.* **28** 4335–8

Sinogeikin S V, Lakshtanov D L, Nicholas J D and Bass J D 2004a. Sound velocity measurements on laser-heated MgO and Al_2O_3 *Phys. Earth Planet. Inter.* **143/144** 575–86

Sinogeikin S V, Zhang J and Bass J D 2004b Elasticity of single crystal and polycrystalline $MgSiO_3$ perovskite by Brillouin spectroscopy *Geophys. Res. Lett.* **2004** L06620-1-5

Wang Y, Weidner D J and Meng Y 1998 *Properties of Earth and Planetary Materials at High Pressure and Temperature* ed M Manghnani and T Yagi (Washington, DC: American Geophysical Union) pp 365–72